Langtaosha (LTS) Preprint doi: https://doi.org/10.65215/LTSpreprints.2026.11.04.000373. This version posted November 4, 2026. The copyright holder for this preprint (which was not certified by peer review) is the author/funder. Creative Commons license: CC Attribution-NonCommercial-NoDerivatives 4.0 https://creativecommons.org/licenses/by-nc-nd/4.0

Scalable and modular synthesis enables pharmacological diversification of salvinorins

Yuyang Ai[1], Jiangwen Gui[3,4], Boxu Lin[1], Min Liu[3,4], Yujun Wang[3,4*], Tuoping Luo[1,2*]

[1]Key Laboratory of Bioorganic Chemistry and Molecular Engineering of Ministry of Education, Beijing National Laboratory for Molecular Science, College of Chemistry and Molecular Engineering, Peking University, Beijing 100871, China, [2]Peking-Tsinghua Center for Life Sciences, Academy for Advanced Interdisciplinary Studies, Peking University, Beijing 100871, China, [3]Shandong Laboratory of Yantai Drug Discovery, Bohai Rim Advanced Research Institute for Drug Discovery, Yantai, Shandong 264117, China; [4]Shanghai Institute of Materia Medica, Chinese Academy of Sciences, Shanghai 201203, China
*Corresponding author: yjwang@simm.ac.cn (Y. W.); tuopingluo@pku.edu.cn (T. L.)

Abstract: Salvinorin A is an atypical opioid characterized by a non-nitrogenous scaffold and potent, selective κ-opioid receptor (KOR) agonistic activity. Its distinctive pharmacology has motivated studies of pain and neuropsychiatric function, but structural complexity and limited synthetic access have constrained mechanistic investigation and pharmacological optimization. Here we report concise and scalable syntheses of EOM-salvinorin B and salvinorin A, together with modular access to 28 new analogs. Temporary skeletal rewiring generates a pyrone that enables photochemical construction of the congested C9 all-carbon quaternary center while directly furnishing a versatile intermediate for diversification at the underexplored C17 position. Notably, C17 substitution yielded potent, selective ligands with distinct signaling bias, binding kinetics and pharmacokinetic behavior. Replacing the C17 carbonyl with an aminomethyl group yielded an ultrapotent analogue with delayed onset and sustained antinociception, contrasting with the rapid, short-lived action of SalA and EOM-SalB, with no locomotor impairment detected under the tested conditions. This work establishes a modular synthetic platform that expands the accessible salvinorin chemical space, providing a foundation for further biological studies.

Langtaosha (LTS) Preprint doi: https://doi.org/10.65215/LTSpreprints.2026.11.04.000373. This version posted November 4, 2026. The copyright holder for this preprint (which was not certified by peer review) is the author/funder. Creative Commons license: CC Attribution-NonCommercial-NoDerivatives 4.0 https://creativecommons.org/licenses/by-nc-nd/4.0

INTRODUCTION

The κ-opioid receptor (KOR), a class A G-protein-coupled receptor (GPCR), is both a promising therapeutic target for pain and mood disorders and a valuable model system for probing GPCR signaling[1]. (–)-Salvinorin A (SalA, **1**; Fig. 1a), first isolated from *Salvia divinorum*[2,3], is a highly potent (EC_{50} = 1.0 – 45 nM across assays) and selective KOR agonist[4,5,6]. Unlike nearly all known opioid ligands, **1** lacks a basic nitrogen atom, a feature associated with high lipophilicity and rapid central nervous system (CNS) penetration[7]. These characteristics establish **1** as an archetypal "atypical" opioid receptor agonist and confer broader utility on the salvinorin chemotype, as illustrated by the use of salvinorin B (**2**; Fig. 1a) in DREADD (designer receptors exclusively activated by designer drugs) systems[8,9], for which high potency, selectivity and CNS penetration are important attributes.

Despite its compelling pharmacology, centrally acting KOR agonists such as **1** are limited by dose-dependent adverse effects, including sedation[10], dysphoria[11,12] and psychotomimetic or hallucinogenic effects[13,14]. Additionally, **1** suffers from poor metabolic stability: the hydrolytically labile C2 acetate drives rapid systemic clearance[15,16]. Over the past two decades, these liabilities have motivated intensive structure–activity relationship (SAR) studies and the preparation of more than 600 semisynthetic SalA analogues (Fig. 1a)[17,18]. Approximately one-third of these derivatives incorporate modifications at the C2 hydroxyl group, yielding candidates such as EOM-SalB (**3**) and MOM-SalB (**4**), which exhibit prolonged plasma half-lives and enhanced potencies[19]. Parallel efforts have focused on modifications to the C12 furan ring; C16 bromo and ethynyl substitutions, for example, led to increased KOR potency and enhanced G-protein signaling bias[20]. Collectively, these studies establish the salvinorin framework as a versatile platform for tuning KOR potency, stability

Langtaosha (LTS) Preprint doi: https://doi.org/10.65215/LTSpreprints.2026.11.04.000373. This version posted November 4, 2026. The copyright holder for this preprint (which was not certified by peer review) is the author/funder. Creative Commons license: CC Attribution-NonCommercial-NoDerivatives 4.0 https://creativecommons.org/licenses/by-nc-nd/4.0

and signalling. Despite these advances, semisynthetic approaches are inherently limited in both the number and diversity of modifiable positions.

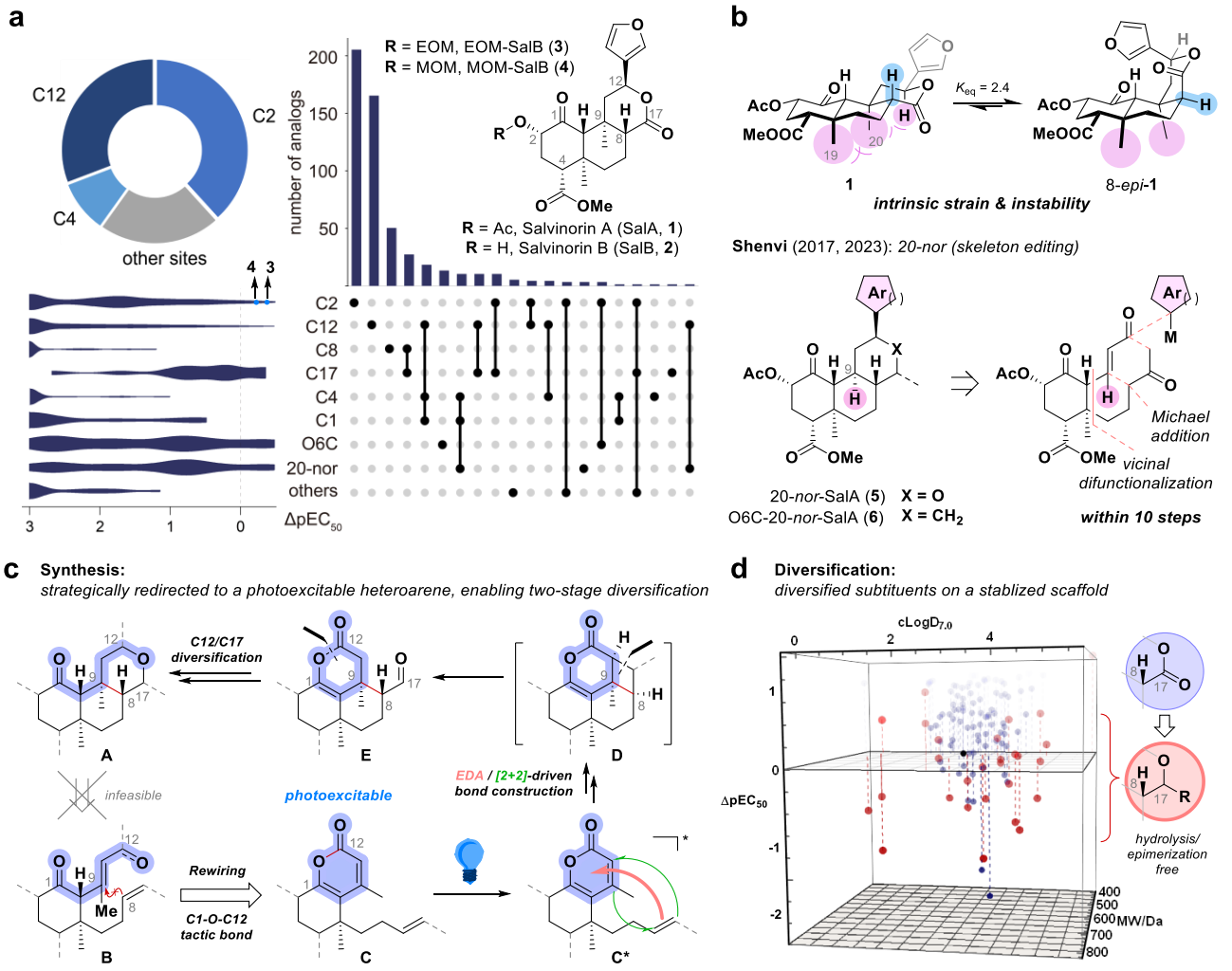


Figure 1. Salvinorin analogue landscape and scaffold design towards modular synthetic diversification. a, An overview of modification sites and the corresponding distribution of potency fold change (ΔpEC_{50} relative to SalA (**1**), for compounds lacking EC_{50} value, ΔpK_i were used) of salvinorin A analogues to date. MOR-selective analogues were not included in this figure. **b,** The problem of destabilizing 1,3-diaxial repulsion between C19 and C20 methyl groups that leads to spontaneous C8 epimerization and complicates synthesis. Excision of C20 methyl simplifies scaffold construction: 20-nor-salvinorin A (**5**), O6C-20-nor-salvinorin A (**6**) and analogues synthesized by Shenvi and coworkers. **c,** A modular and efficient synthesis of salvinorins leverages a photoexcitable pyrone intermediate to forge the challenging C–C bond. **d**, Synthetic modularity enabled the discovery of analogues with potent and diversified properties (red dots, this work) in comparison to known salvinorin analogues (purple dots).

Langtaosha (LTS) Preprint doi: https://doi.org/10.65215/LTSpreprints.2026.11.04.000373. This version posted November 4, 2026. The copyright holder for this preprint (which was not certified by peer review) is the author/funder. Creative Commons license: CC Attribution-NonCommercial-NoDerivatives 4.0 https://creativecommons.org/licenses/by-nc-nd/4.0

De novo synthesis offers access beyond these restrictions. However, existing total and formal syntheses remain lengthy (16–32 linear steps), low-yielding (0.22%–1.7%)[21–28] and have not generally been demonstrated on preparative scale (Fig. S1). These difficulties stem largely from the intrinsic instability of the *trans*-fused *neo*-clerodane core, which experiences severe diaxial strain between the C19 and C20 methyl groups and readily undergoes epimerization at C8[29] (Fig. 1b). Shenvi and co-workers improved synthetic tractability and scaffold stability by deleting the C20 methyl group (Fig. 1b, **5** and **6**)[29,30]. Further diversification furnished a series of potent, selective and biased 20-nor analogues, underscoring the value of deep-seated structural modifications for salvinorin-based pharmacological explorations[30].

Recent structural biology advances have provided unprecedented insight into salvinorin-KOR engagement. Cryo-EM structures of KOR–G-protein complexes bound to **4**[31] or **1**[32] revealed a predominant hydrophobic interaction network[33] and rationalized prior mutagenesis data implicating residues in ligand affinity, selectivity and bias[34,35], thereby guiding structure-based salvinorin modification. Our examination of these reported structures identified the C17 carbonyl, directed towards the extracellular vestibule, as a promising diversification site (*vide infra*). We reasoned that substituents introduced here could vary in charge, polarity and size while preserving the core ligand–receptor contacts, thereby providing a complementary modulation vector to the established SAR at C2 and C12.

We therefore sought a concise, scalable synthesis that would enable systematic diversification of the salvinorin scaffold (**A**, Fig. 1c). A central synthetic challenge lies in addressing the kinetic and thermodynamic barriers associated with C8–C9 bond formation (and construction of the C9 all-carbon quaternary center) in intermediates resembling **B**, which have thus far been accessible only through a 14-membered ring transannular cyclization[21] or following C20 methyl deletion[29,30]. To surmount these intrinsic barriers, we strategically rewired the molecular framework into pyrone **C**, introducing the counterintuitive C1–O/C12 linkage as a “tactic bond” that generates a photoexcitable heterocycle. Upon irradiation, access to the excited state (**C***) enables the otherwise unfavorable C8–C9 bond formation to furnish **E** via **D**. Equally importantly, this design directly furnishes **E** with a

Langtaosha (LTS) Preprint doi: https://doi.org/10.65215/LTSpreprints.2026.11.04.000373. This version posted November 4, 2026. The copyright holder for this preprint (which was not certified by peer review) is the author/funder. Creative Commons license: CC Attribution-NonCommercial-NoDerivatives 4.0 https://creativecommons.org/licenses/by-nc-nd/4.0

versatile aldehyde handle, predisposing the scaffold to efficient downstream C17 and C12 modular diversification and thereby unlocking rapid access to analogues spanning distinct physicochemical and pharmacological profiles (Fig. 1d).

RESULT AND DISCUSSION

We selected EOM-SalB (**3**), rather than **1**, as the initial target because its C2 substituent confers greater potency and stability[36]. Guided by the *excitable-pyrone* retrosynthetic analysis, we initiated the synthesis from enantiopure 2-hydroxy-Hagemann's ester (**7**), previously established by Shenvi and co-workers (Fig. 2a)[30]. Ethoxymethylation with 2-pySEOM (**8**) in the presence of AgOTf and NaOAc furnished enone **9** in 97% yield[37]. Conjugate addition of Grignard reagent **10** to **9** generated the corresponding silyl enol ether with excellent diastereoselectivity, which upon treatment with TMS-EBX and TBAF at –78 °C afforded allene **11** in 62% yield over two steps following *in situ* isomerization[38]. The hetero-Diels–Alder reaction of **11** with **12**[39]**,** followed by a desilylation–aromatization sequence, provided **13** in 78% yield on a 4 g scale. Subsequent olefin cross-metathesis with **14** furnished pinacol borate **15** in 72% yield. A pyrone–alkene [2+2] cycloaddition was realized using a phenothiazine photocatalyst (**PTH**) under 410 nm irradiation in DMSO, delivering boryl cyclobutane **16** in >90% NMR yield, consistent with photosensitization that suppresses singlet-state pyrone photoelectrocyclization[40]. *In situ* oxidation of **16** with **17** triggered spontaneously *retro*-aldol cleavage and C8 epimerization, presumably catalyzed by $PhNMe_2$ generated *in situ*, affording aldehyde **18** with the desired C8 configuration in 77% isolated yield on a 3 g scale. Notably, an alternative protocol involving irradiation of the *in situ*-formed enamine **19** (Fig. 3a) also delivered **18**; mechanistic experiments supported an electron donor–acceptor (EDA) complex mechanism (Fig. 3b–d), underscoring the robustness of photochemical strategies for challenging bond formations (Fig. S1d).

Aldehyde **18** was transformed into lactol **20** via redox operations. Screening of acid catalysts revealed that diphenylphosphoric acid [$(PhO)_2OPOH$] efficiently promoted translactolization of **20** to **22** in dichloromethane, achieving an approximate 6:1 product-to-starting-material ratio at equilibrium. In THF, toluene or acetonitrile the equilibrium instead favored **20**,

Langtaosha (LTS) Preprint doi: https://doi.org/10.65215/LTSpreprints.2026.11.04.000373. This version posted November 4, 2026. The copyright holder for this preprint (which was not certified by peer review) is the author/funder. Creative Commons license: CC Attribution-NonCommercial-NoDerivatives 4.0 https://creativecommons.org/licenses/by-nc-nd/4.0

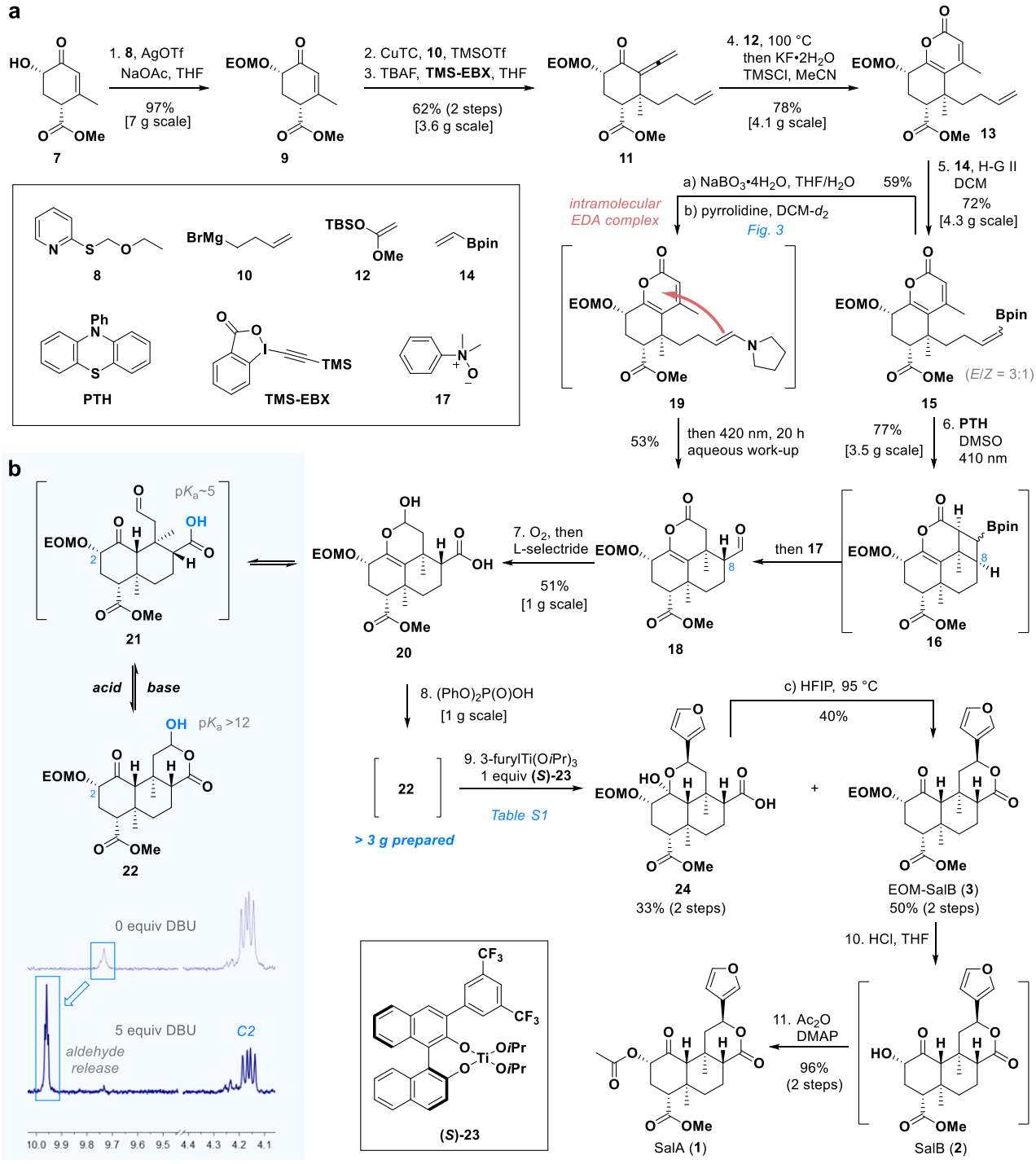


Figure 2. Total synthesis of (–)-EOM-SalB and (–)-SalA. **a,** The complete synthesis of EOM-SalB and SalA via a pyrone-[2+2] approach is shown. Step number is indicated by the numbers before the reaction conditions. **b,** The equilibrium between **20** and **22** via **21** as evidenced by *in situ* NMR

whereas weaker and stronger acids gave poor conversion or decomposition. These solvent and acidity effects are consistent with a finely balanced equilibrium mediated through intermediate **21** (Fig. 2b).

Langtaosha (LTS) Preprint doi: https://doi.org/10.65215/LTSpreprints.2026.11.04.000373. This version posted November 4, 2026. The copyright holder for this preprint (which was not certified by peer review) is the author/funder. Creative Commons license: CC Attribution-NonCommercial-NoDerivatives 4.0 https://creativecommons.org/licenses/by-nc-nd/4.0

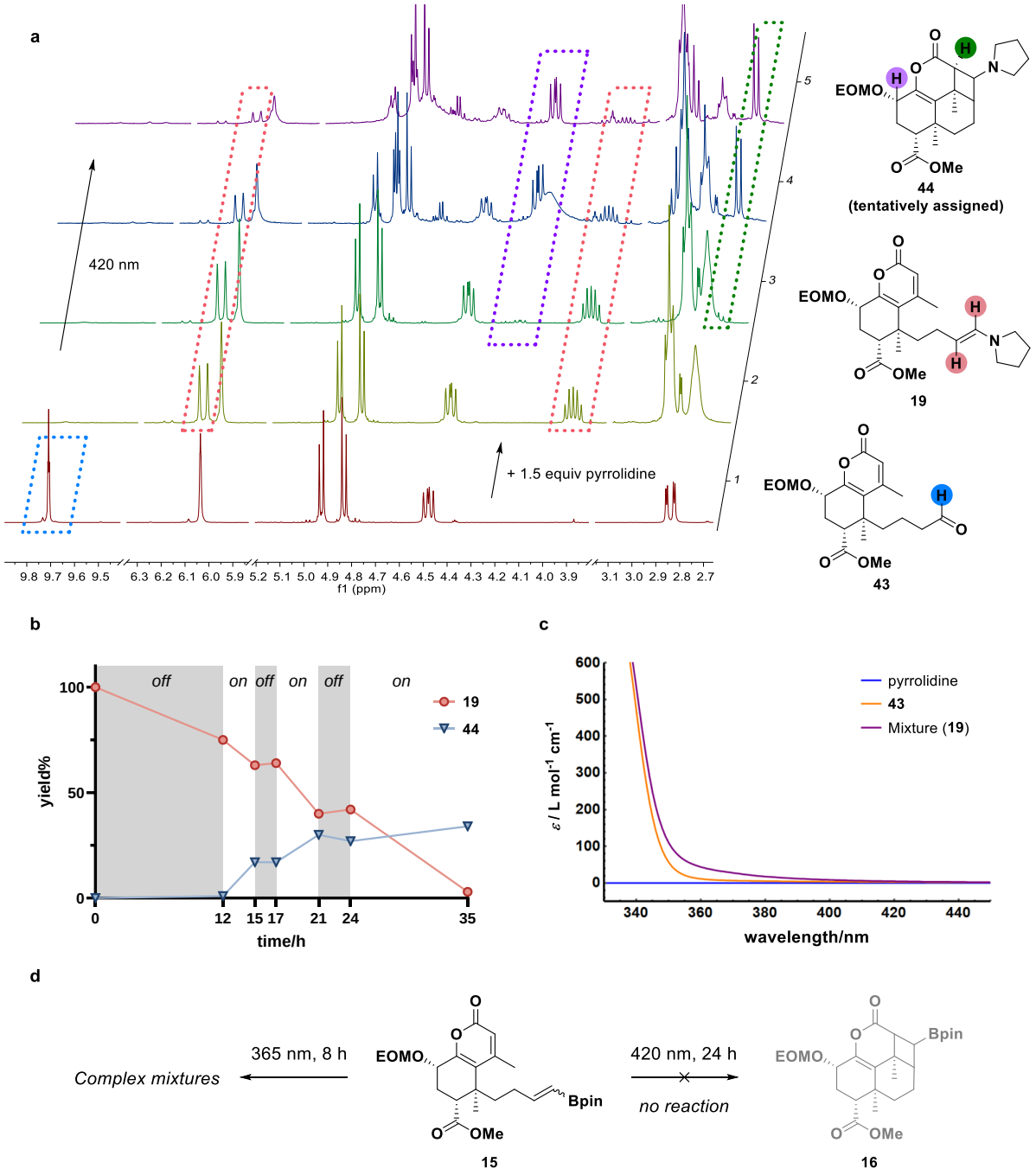


Figure 3. Synthesis of 18 via an EDA complex approach. (**a**) Reaction monitored by *in situ* NMR. Addition of pyrrolidine to **43** gave a clear signal of *trans*-enamine **19** (y-axis, 1 to 2), subsequent irradiation (y-axis, 3: 1 h, 4: 14 h, 5: 24 h) yielded a set of new signals (**44**), which upon work-up afforded **18**. (**b**) Light on/off experiment did not support a ground-state mechanism (**c**) UV-vis spectra supported formation of an EDA complex. (**d**) Control experiments on **15** showed the pyrone was not excitable under 420 nm; direct excitation of pyrone yielded complex products.

With a concise and gram-scale route to **22** established, we next pursued its conversion to EOM-SalB (**3**). Attempts at deoxygenative cross-coupling on **22** were evaluated (Fig. S2).

Langtaosha (LTS) Preprint doi: https://doi.org/10.65215/LTSpreprints.2026.11.04.000373. This version posted November 4, 2026. The copyright holder for this preprint (which was not certified by peer review) is the author/funder. Creative Commons license: CC Attribution-NonCommercial-NoDerivatives 4.0 https://creativecommons.org/licenses/by-nc-nd/4.0

However, the equilibration between **21** and **22** suggested that a nucleophilic addition strategy targeting intermediate **21** could provide an alternative entry. Reacting **22** with 3-furyltitanium[24,41] afforded (–)-EOM-SalB (**3**) and **24** in high combined yield after acidic workup, but favored the undesired diastereomer. Incorporation of a BINOL-chelated chiral Lewis acid (*S*)-**23**[42] and lowering the reaction temperature significantly improved selectivity, delivering EOM-SalB (**3**) in 50% yield over two steps from **20** without detectable C8 epimerization, along with 33% of **24** (Table S1). Notably, heating **24** in HFIP enabled its conversion to **3** in moderate yield. The identity and enantiopurity of **3** were further confirmed via a two-step transformation to (–)-salvinorin A (**1**), whose spectroscopic properties and optical rotation matched reported values (Fig. S3).

Overall, we achieved a protecting-group-free total synthesis of EOM-SalB (**3**) in 7% overall yield over 9 steps from **7**. Across multiple batches, this route has furnished more than 15 g of **18** and more than 3 g of **22**. This scalable and efficient strategy for the synthesis of salvinorins (Fig. S1) laid the foundation for subsequent functional diversification.

The two principal shortcomings of **1**—its poor pharmacokinetics and undesirable central side-effects—represent key challenges we sought to address. Guided by the cryo-EM structure of **4**-bound KOR[31], we aimed to streamline analogue design by pinpointing structurally permissive modification sites. The most extensively explored positions (C2, C4, and C12) are deeply buried within the compact binding pocket, where they engage in stabilizing hydrophobic interactions with the receptor (Fig. 4a). This structural constraint likely explains why only small, hydrophobic substituents (e.g., the EOM group at C2 or the ethynyl group at C16) enhance potency relative to **1**. In contrast, the C17 carbonyl group is oriented toward the extracellular vestibule of KOR, a cavity capable of accommodating bulky functional groups without disrupting core receptor–ligand interactions[43]. Such substitutions could also contact extracellular loop 2 (ECL2), which has been implicated in GPCR ligand bias[44,45] and binding kinetics[46]. Moreover, converting the C17 lactone into a tetrahydropyran was also expected to avoid C8 epimerization and lactone hydrolysis (Fig. 4b). Collectively, C17 substitution therefore provides an opportunity for fine-tuning pharmacological profiles while

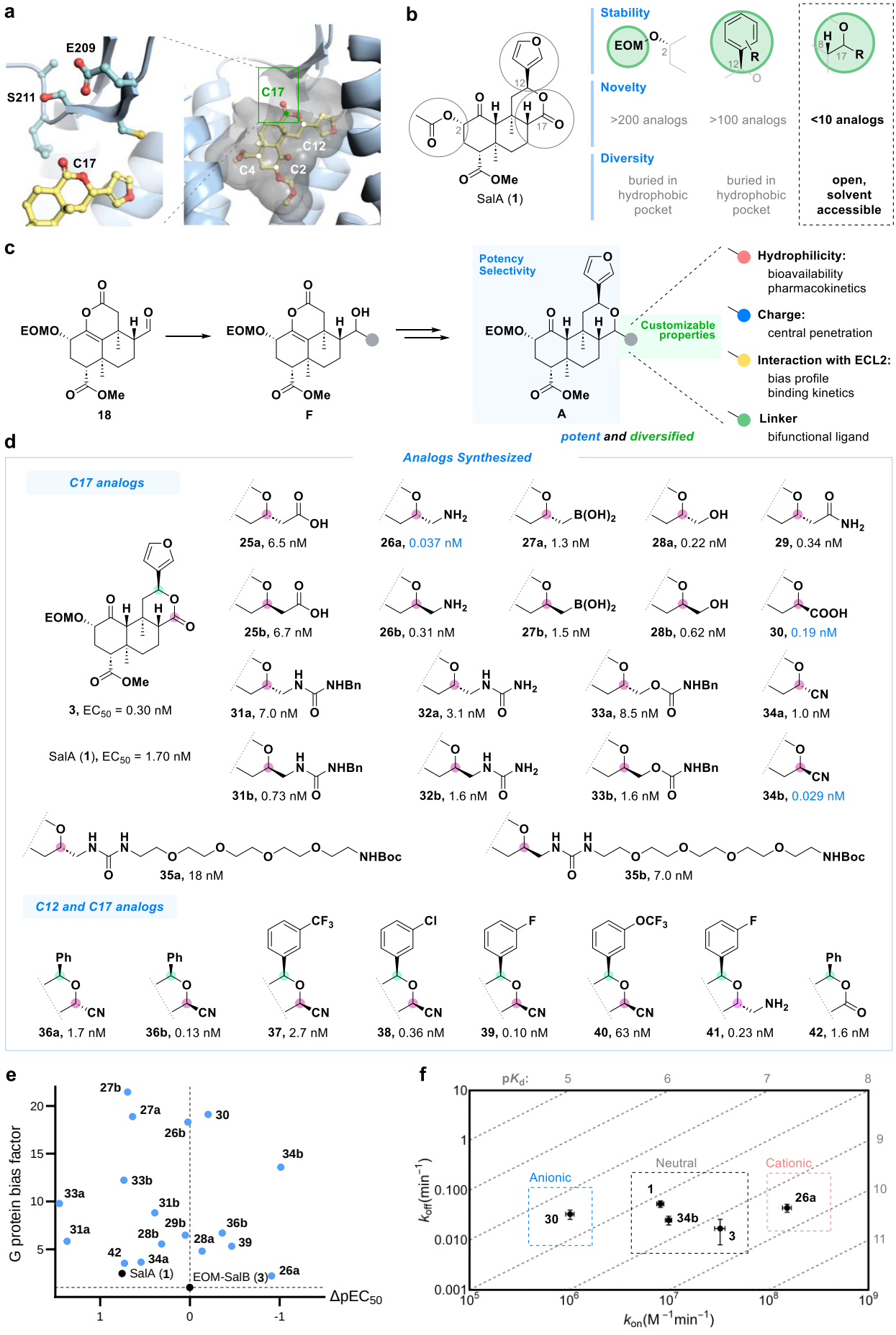
Langtaosha (LTS) Preprint doi: https://doi.org/10.65215/LTSpreprints.2026.11.04.000373. This version posted November 4, 2026. The copyright holder for this preprint (which was not certified by peer review) is the author/funder. Creative Commons license: CC Attribution-NonCommercial-NoDerivatives 4.0 https://creativecommons.org/licenses/by-nc-nd/4.0

preserving KOR potency and selectivity, yielding a diversified yet potent analogue library. Notably, such C17-modified salvinorin analogues have been scarcely explored (Fig. 1a and Fig. 4b), whereas our synthetic strategy enables their efficient preparation from a versatile intermediate **F,** derived from **18**, allowing access to both diastereomers (Fig. 4c).

A four-step sequence furnished carboxylic acids **25a** and **25b** as versatile diversification precursors (Fig. S4). *In vitro* cAMP inhibition assays revealed that both compounds exhibited an approximately 20-fold reduction in potency relative to **3** (Fig. 4d and Table S2), establishing a benchmark for subsequent optimization. We next diversified the C17 carboxymethyl group into a range of small, hydrophilic substituents to probe potential interactions with ECL2. Boronic acid derivatives **27a** and **27b**, designed to form reversible covalent interactions[47] with $S211^{ECL2}$, displayed moderate potency. Inspired by the canonical amine pharmacophore of opioid ligands and the distinct physicochemical properties conferred by basic amines, we next introduced amino substituents at C17. Interestingly, both aminomethyl analogues retained high potency, and the α-aminomethyl analogue **26a** was eightfold more potent than **3** in the cAMP assay (EC_{50} = 0.037 nM). Notably, in terms of ligand lipophilicity efficiency[48] (LLE, calculated here as pEC_{50}-$cLogD_{7.4}$), **26a** achieved an exceptional LLE of 10.1, compared with 6.5 for EOM-SalB, with potential benefits for solubility and reduced lipophilicity-related off-target risks[48,49].

Further functionalization of the hydroxyl and amino groups afforded a series of analogues, in which a stereochemical trend emerged: C17α-analogues were generally more potent than their β-epimers when bearing small, hydrophilic substituents (e.g., **26a** and **28a**), whereas C17β-analogues became favoured as the substituent size increased (e.g., **31b**, **32b**, and **35b**). This trend suggests that the β-configuration may better accommodate linker attachment or further pharmacophore expansion.

Langtaosha (LTS) Preprint doi: https://doi.org/10.65215/LTSpreprints.2026.11.04.000373. This version posted November 4, 2026. The copyright holder for this preprint (which was not certified by peer review) is the author/funder. Creative Commons license: CC Attribution-NonCommercial-NoDerivatives 4.0 https://creativecommons.org/licenses/by-nc-nd/4.0



Langtaosha (LTS) Preprint doi: https://doi.org/10.65215/LTSpreprints.2026.11.04.000373. This version posted November 4, 2026. The copyright holder for this preprint (which was not certified by peer review) is the author/funder. Creative Commons license: CC Attribution-NonCommercial-NoDerivatives 4.0 https://creativecommons.org/licenses/by-nc-nd/4.0

Figure 4. Design and synthesis of salvinorin C17 analogues. **a,** Right, MOM-SalB (**4**) in the binding pocket of KOR identified in ref 31. The C17 substituents point towards the exterior of the orthosteric site. Left, C17 substituents may engage in polar interactions with residues on ECL2. **b,** Based on the binding pose, KOR was hypothesized to accommodate a wide range of C17-substituted salvinorins with minimal effects on affinity. Diversifications at C17 would potentially generate a library of stabilized, novel and divergent salvinorin analogues. **c,** An efficient and modular route from key intermediate **18** to C12 and C17 salvinorin analogues was established. **d,** Focused library synthesized in this study. **e,** The bias and potency profile of representative analogues. **f,** Binding parameters for representative analogues. Differences in K_i were primarily driven by variations in k_{on}.

The nitrile functional group is a well-established carbonyl mimic in medicinal chemistry[50,51]. To access C17 nitrile analogues, the primary alcohol in **28b** was oxidized to yield carboxylic acid **30**, a potent anionic KOR agonist (EC_{50} = 0.19 nM). Subsequent amidation and dehydration furnished nitrile **34b** (EC_{50} = 0.029 nM), displaying an order-of-magnitude increase in potency relative to **3**.

The potency of **34b** also provided a basis for C12 diversification, motivated by concerns regarding oxidative metabolism–induced hepatotoxicity associated with furyl groups[52]. The synthesis of **34b** was streamlined to four steps from aldehyde **18** (Fig. S5). Guided by SAR studies of the aryl substituents in nalfurafine[53]—whose binding mode, particularly involving the furan ring, closely resembles that of **4** (Fig. S6)—and salvinorins[29,30], several C12 substituted analogues (**36**–**42**) were synthesized in a modular manner. Among these, the 3-fluorophenyl derivative **39** was the most potent. The phenyl analogue **36b** also maintained high potency, whereas bulkier substituents on the phenyl ring led to diminished activity, consistent with a tight lipophilic pocket around C12[30]. The corresponding C17α-nitrile analogues (**34a** and **36a**) exhibited reduced potency, in line with their altered orientation relative to the native lactone carbonyl.

Encouragingly, 26 out of 28 analogues retained single-digit-nanomolar potency (Fig. 4d). Representative compounds also exhibited excellent selectivity over MOR and DOR (Fig. S7), consistent with the spatial separation of the selectivity-determining residue V108$^{2.53}$ (Ballesteros–Weinstein numbering[54]) from the C17 substitution site. Signalling bias studies revealed notable trends: epimers **26a** and **26b** displayed markedly different G-protein bias, potentially arising from additional interactions of **26b** within the TM5/ECL2 subpocket[45]. In

Langtaosha (LTS) Preprint doi: https://doi.org/10.65215/LTSpreprints.2026.11.04.000373. This version posted November 4, 2026. The copyright holder for this preprint (which was not certified by peer review) is the author/funder. Creative Commons license: CC Attribution-NonCommercial-NoDerivatives 4.0 https://creativecommons.org/licenses/by-nc-nd/4.0

contrast, **27a** and **27b** consistently exhibited high G-protein bias. Although nitrile **34b** was initially designed to mimic the interaction profile of **3**, it displayed substantially enhanced G-protein bias (Fig. 4e). These observations corroborated prior findings on 20-*nor*-salA,[30] highlighting the impact of C17 modifications on functional selectivity.

Among all analogues, it was noteworthy that **26a**, **30**, and **34b**—despite differing in net charge—each exhibited exceptional potency. To better understand these observations, we measured their binding kinetics and affinities, which reflect the underlying ligand-receptor interactions (Fig. 4f and Fig. S8). While all compounds displayed comparable dissociation rates (k_{off}), their association rates (k_{on}) spanned nearly three orders of magnitude and followed a charge-dependent trend. Association was fastest for positively charged **26a**, intermediate for neutral **1**, **3** and **34b**, and slowest for the anionic **30**, consistent with an electrostatic contribution to ligand association at the negatively charged extracellular domain of KOR[55,56]. Binding affinity followed the same charge-dependent rank order (Table S2). Molecular dynamics (MD) simulations were performed to further elucidate potential interactions in the orthosteric pocket. The simulations revealed that C17 substituents of **26a**, **30** and **34b** formed additional polar interactions while preserving the core hydrophobic stabilization of the scaffold (Fig. S9a-c). Specifically, the protonated amino group of **26a** formed a persistent salt bridge with $E209^{ECL2}$ (observed in >50% simulation frames over three 1,000-ns replicates). In the case of **34b**, the nitrile group engaged in hydrogen bonding with the backbone amide of $L212^{ECL2}$ (>75% of frames), exceeding that observed for **3** (<40% of frames). For the anionic analogue **30**, a frequently observed salt bridge with $K227^{5.40}$ (>60% of frames)—a residue implicated in KOR signalling bias—may account for its observed G-protein bias profile. MM-PBSA calculations also identified favorable energetic contributions from these residues (Fig. S9d).

Collectively, these data provide mechanistic support for the C17 derivatization strategy, demonstrating that tailored polar modifications can modulate KOR signaling bias and binding kinetics while preserving the core hydrophobic interaction network of the salvinorin scaffold.

Langtaosha (LTS) Preprint doi: https://doi.org/10.65215/LTSpreprints.2026.11.04.000373. This version posted November 4, 2026. The copyright holder for this preprint (which was not certified by peer review) is the author/funder. Creative Commons license: CC Attribution-NonCommercial-NoDerivatives 4.0 https://creativecommons.org/licenses/by-nc-nd/4.0

We next examined whether these structural modifications of salvinorin translated into distinct pharmacological effects *in vivo*. To this end, **26a**, **30**, and **34b** were evaluated in a mouse hot-plate antinociception assay (Fig. 5a–c). Compounds were initially compared at 2 mg/kg, a dose close to the reported antinociceptive ED_{50} of **1**[57]. As expected, SalA (**1**) exhibited its characteristic rapid onset and clearance, while EOM-SalB (**3**), despite its greater potency, displayed similarly transient activity. Remarkably, **34b** produced a stronger antinociceptive effect, achieving 90% maximum possible effect (MPE) within 20 min at the same dose. At 1 mg/kg, **34b** elicited a MPE comparable to that of morphine (10 mg/kg) at 20 min, but the effect rapidly declined to baseline within 1 h, as observed for **1** and **3**.

Conversely, the cationic analogue **26a** exhibited a markedly different pharmacodynamic profile. Its antinociceptive effect developed gradually, became apparent at approximately 1 h post-injection, reached its maximum at 4–6 h and returned to baseline after 9 h, indicating a substantially longer duration than those of **1**, **3** and **34b** under the tested conditions. In contrast, the anionic analogue **30** showed no detectable activity in the hot-plate assay but significantly attenuated acetic acid-induced writhing (Fig. 5d), consistent with peripherally restricted KOR agonism[58], possibly as a consequence of the negative charge[59,60].

Having established that **34b** and **26a** effectively elicited central antinociception, we next investigated whether these centrally active analogues produced sedative-like effects (Fig. 5e). In the open-field test, administration of **34b** significantly reduced spontaneous locomotion, whereas **26a** produced no detectable locomotion impairment. Consistently, **26a** did not impair rotarod performance (Fig. 5f).

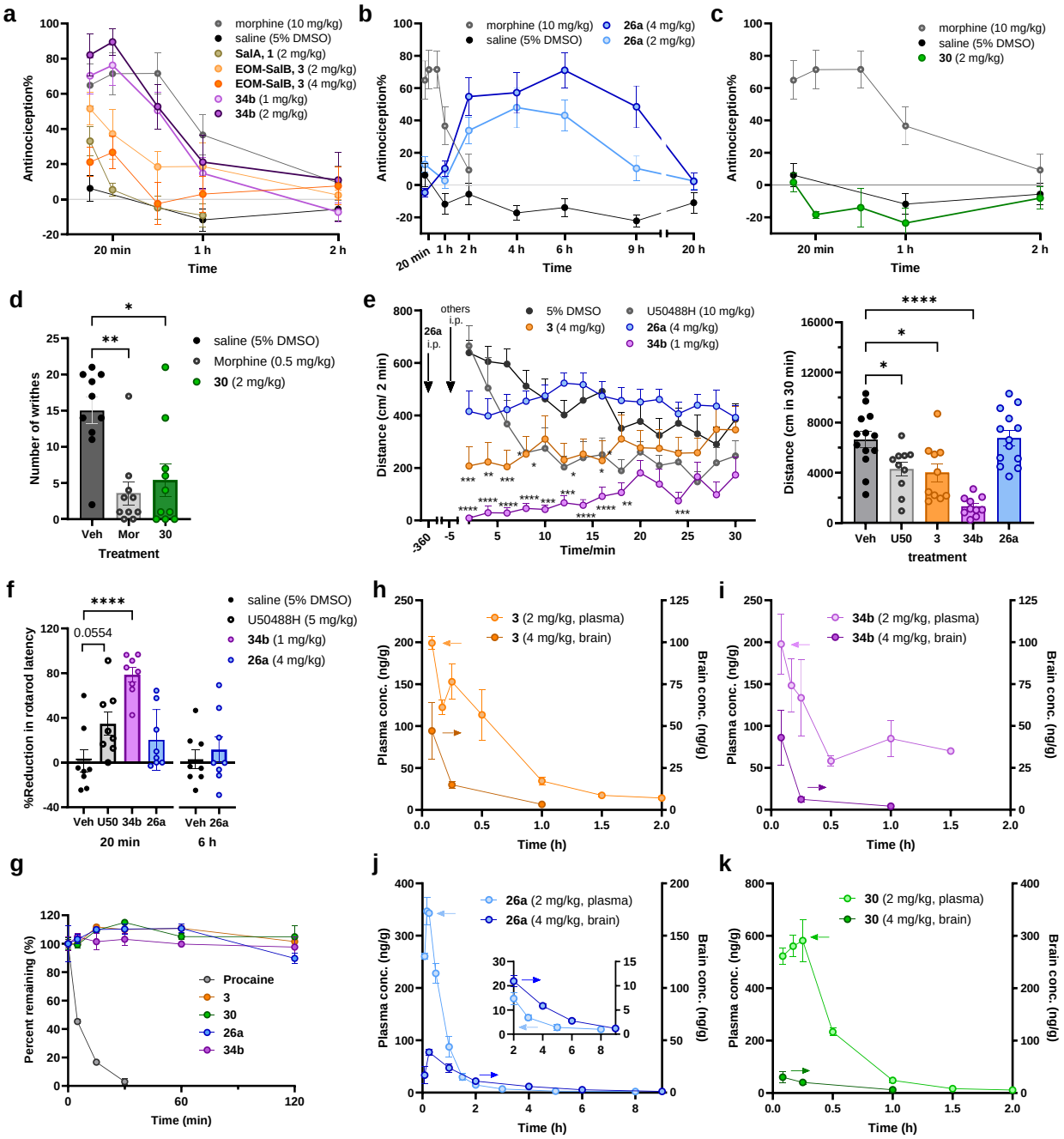
We next compared the pharmacokinetic properties of **26a** and **34b** to investigate their different *in vivo* pharmacodynamics. To this end, key pharmacokinetic parameters were evaluated (Table S3, Fig. 5g–k). The metabolic stabilizing effect of the EOM-substituent was first validated, as all tested compounds remained stable during the 2 h plasma incubation (Fig. 5g). In the MDCK-MDR1 bidirectional permeability assay (Table S3), the neutral compounds (**1**, **3** and **34b**) displayed high permeability and were insensitive to active transport, whereas the charged analogues (**30** and **26a**) exhibited high efflux ratios,

Langtaosha (LTS) Preprint doi: https://doi.org/10.65215/LTSpreprints.2026.11.04.000373. This version posted November 4, 2026. The copyright holder for this preprint (which was not certified by peer review) is the author/funder. Creative Commons license: CC Attribution-NonCommercial-NoDerivatives 4.0 https://creativecommons.org/licenses/by-nc-nd/4.0

particularly **26a**. This observation was unexpected given the potent antinociceptive activity of **26a** in the hot-plate assay.

The *in vivo* pharmacokinetic studies revealed similar plasma half-lives but different systemic exposures across the compounds: the more hydrophilic analogues **30** and **26a** reached higher plasma C_{max} and AUC values (Fig. 5j–k). As anticipated, **3** and **34b** exhibited rapid brain penetration and elimination, with brain exposure closely paralleling plasma levels (Fig. 5h–i). Consistent with the MDCK-MDR1 permeability assay and its lack of activity in the hot-plate assay, **30** had a low brain/plasma ratio over the sampled interval, supporting peripheral restriction (Fig. 5k). Both plasma and brain concentrations of **26a** peaked at 15 min, when the dose-normalized brain-to-plasma ratio was about 1:18. Thereafter, by 2 h post-administration, the brain-to-plasma ratio increased to approximately 1:3, and measurable brain concentrations persisted for at least 9 h (Fig. 5j). In addition, a pronounced pharmacokinetic-pharmacodynamic hysteresis[61] was observed, as demonstrated by the delayed onset of maximal antinociception relative to peak brain concentration. Interestingly, these features resemble those reported for JDTic, suggesting a potentially similar explanation[61]: Efflux may limit the initial brain exposure of **26a**, thereby reducing centrally mediated adverse effects. Following entry into the CNS, **26a** may redistribute slowly and accumulate in KOR-rich regions, contributing to its delayed onset of action. Together, its sub-nanomolar potency, rapid association kinetics[62], along with the propensity of positively charged compounds for nonspecific tissue binding or lysosomal sequestration[63], may account for its sustained *in vivo* activity. These findings establish C17 as a privileged site for expanding the accessible chemical and pharmacological space of the salvinorin scaffold.

Langtaosha (LTS) Preprint doi: https://doi.org/10.65215/LTSpreprints.2026.11.04.000373. This version posted November 4, 2026. The copyright holder for this preprint (which was not certified by peer review) is the author/funder. Creative Commons license: CC Attribution-NonCommercial-NoDerivatives 4.0 https://creativecommons.org/licenses/by-nc-nd/4.0



268

Langtaosha (LTS) Preprint doi: https://doi.org/10.65215/LTSpreprints.2026.11.04.000373. This version posted November 4, 2026. The copyright holder for this preprint (which was not certified by peer review) is the author/funder. Creative Commons license: CC Attribution-NonCommercial-NoDerivatives 4.0 https://creativecommons.org/licenses/by-nc-nd/4.0

Figure 5. Pharmacological effects of selected salvinorin analogues. **a,** Compared with SalA (**1**) and EOM-SalB (**3**), **34b** produced greater maximal antinociceptive activity, but were similar in the short duration of action in the hot-plate test ($N = 9$ mice for vehicle, 2 mg/kg **3**, 4 mg/kg **3** and 2 mg/kg **34b** treatments; $N = 10$ mice for all other treatments). **b, 26a** had slower onset rate but prolonged duration of action, extending over 9 hours ($N = 9$ mice for vehicle; $N = 10$ mice for all other treatments). **c, 30** did not produce detectable antinociception in hot-plate test ($N = 9$ mice for vehicle; $N = 10$ mice for morphine; $N = 5$ mice for **30**). **d, 30** significantly diminished acetic acid-induced writhing ($N = 10$ mice for all treatments); Kruskal–Wallis test with Dunn's multiple-comparisons test as compared to the Veh control (Veh versus morphine (Mor), $P = 0.0049$; Veh versus **30**, $P = 0.0164$). Data are presented as mean ± s.e.m. **e,** Sedative-like effects were assessed by spontaneous locomotor activity (distance per 2 min, left; total distance, right) in the open field test. EOM-SalB (**3**) was effective in reducing locomotor activity while **34b** markedly inhibited the locomotor activity. **26a** did not show detectable sedative-like effects ($N = 13$ mice for vehicle (Veh) and **26a** treatment; $N = 10$ mice for all other treatments). Vehicle, U50488H, **3** and **34b** were tested 5 min after injection, whereas **26a** was tested after 6 h; The time-course data (left) were analyzed using two-way repeated-measures analysis of variance (ANOVA) with the Geisser–Greenhouse correction, with treatment as the between-subject factor and time as the within-subject factor, followed by Dunnett's multiple-comparisons test comparing each treatment with vehicle at each time point. Total distance (right) was analyzed using one-way ANOVA with Dunnett's post hoc test as compared to the Veh control (Veh versus U50488H (U50), $P = 0.0256$; Veh versus EOM-SalB (**3**), $P = 0.0102$; Veh versus **34b**, $P < 0.001$; Veh versus **26a**, $P = 0.9996$). Data are presented as mean ± s.e.m. **f,** Compounds were tested at 20 min post-injection in rotarod test, and again at 6 h post-injection for vehicle and **26a**. **26a** displayed no detectable sedative-like effect. Data are presented as mean ± s.e.m. The 20 min data were analysed using ordinary one-way ANOVA with Dunnett's post hoc test as compared to the Veh control (Veh versus U50488H (U50), $P = 0.0554$; Veh versus **34b**, $P < 0.0001$; Veh versus **26a**, $P = 0.4325$). The 6 h comparison was analysed using a two-sided unpaired *t*-test ($P = 0.1981$). ($N = 8$ mice for all treatments) **g,** EOM-protected compounds showed high *in vitro* plasma stability ($N = 2$ wells from one experiment for all compounds). **h-k,** *In vivo* plasma and total brain concentration curves after *i.p.* administration of **3** (**h**), **34b** (**i**), **26a** (**j**) and **30** (**k**). Plasma concentrations were measured after 2 mg/kg and brain concentrations after 4 mg/kg ($N = 3$ mice per timepoint for all treatment). *$P < 0.05$, **$P < 0.01$, ***$P < 0.001$, ****$P < 0.0001$.

CONCLUSION

Salvinorins remain an incompletely explored class of opioid receptor ligands[64], and access to SalA (**1**) and SalB (**2**) still relies largely on natural sources[65,66]. Broader exploration of this chemotype has been hindered by structural complexity and by the inefficiency and limited derivatization capacity of existing synthetic routes (Fig. S1). Recent advances, exemplified by the exploration of 20-*nor*-salvinorins by Shenvi and co-workers[29,30], have begun to address these challenges. Here, we disclose a concise and scalable total synthesis of EOM-SalB (**3**)

Langtaosha (LTS) Preprint doi: https://doi.org/10.65215/LTSpreprints.2026.11.04.000373. This version posted November 4, 2026. The copyright holder for this preprint (which was not certified by peer review) is the author/funder. Creative Commons license: CC Attribution-NonCommercial-NoDerivatives 4.0 https://creativecommons.org/licenses/by-nc-nd/4.0

that improves synthetic accessibility to salvinorins (Fig. 2). Central to our synthesis is intermediate **18**, generated through excited-state reactions of a strategically introduced pyrone while preserving a synthetically versatile aldehyde as a privileged diversification handle (Fig. 4). This approach embodies an unconventional pyrone-centered "tactical combination[67]" and, more broadly, illustrates how strategic intermediate design can simultaneously enhance synthetic tractability and diversification potential. Such principles may prove broadly useful for developing efficient syntheses of diverse structurally complex targets.

Consistent with insights from cryo-EM structural studies, the C17 position accommodates a broad range of substituents with varied size and charge. Beyond conventional potency and selectivity metrics, increasing evidence highlights drug spatiotemporal distribution as a critical determinant of signaling outcomes[68,69]. Likewise, ligand-binding kinetics can influence signaling bias[70], pharmacokinetic behavior[71] and safety profiles[72]. Our findings identify C17 as an effective molecular handle for tuning these properties. Strategic modification at C17 altered the molecular pharmacology and pharmacokinetic behavior of salvinorins and, for selected analogues, reshaped the observed pharmacodynamic profiles. Negatively charged **30** was peripherally-biased, which was expected to minimize centrally mediated adverse effects[73]. Meanwhile, **26a** exhibited potent antinociceptive activity with minimal sedative-like effects and prolonged duration of action. Pharmacokinetic analyses indicate that **26a** achieved appreciable brain exposure and displayed prolonged brain retention.

Beyond antinociception, it will be interesting to determine how tailored C17 modifications influence the profound psychoactive effects of SalA[14]. Such studies may not only facilitate the use of salvinorin with reduced neuropsychiatric liabilities, but could also provide a foundation for salvinorin-derived neuropsychiatric therapeutics[74].

ASSOCIATED CONTENT

Supporting information

Langtaosha (LTS) Preprint doi: https://doi.org/10.65215/LTSpreprints.2026.11.04.000373. This version posted November 4, 2026. The copyright holder for this preprint (which was not certified by peer review) is the author/funder. Creative Commons license: CC Attribution-NonCommercial-NoDerivatives 4.0 https://creativecommons.org/licenses/by-nc-nd/4.0

All data is made available in the main text, the Supporting Information or the Source Data file, including experimental procedures, additional figures and tables, copies of NMR spectra, MD simulation data and files, all pharmacological protocols and raw data.

Acknowledgements

This work was supported by the National Natural Science Foundation of China (Grants 22425101 and 22171011), College of Chemistry and Molecular Engineering, Peking University, Beijing National Laboratory for Molecular Sciences, Peking-Tsinghua Center for Life Sciences, and Shenzhen Bay Laboratory. We thank Prof. Chen Song (Peking University) and Prof. Ryan Shenvi (Scripps Research Institute) for helpful discussions. The measurements of NMR and mass spectrometry were performed at the Analytical Instrumentation Center of Peking University. We acknowledge the assistance and support from PKUAIC and support from the High-Performance Computing Platform of Peking University. The authors acknowledge the use of ChatGPT (OpenAI) for assistance in language refinement.

Author contributions

The overall design of this project was conceptualized by Y.A., Y.W. and T.L.; Y.A. and B.L. conducted the chemical experiments. Y.A. and J.G. conducted the animal experiments and radioligand binding assays. Y.A. and M.L. performed the cell-based assays. Y.A. performed the molecular dynamics simulations. The manuscript was written and edited jointly by Y.A., Y.W. and T.L. with feedback from other authors.

Declaration of interests

T.L., Y.W., Y.A., B.L., M.L. and J.G. are inventors on a pending Chinese patent application (Application No. 2026110765089) and a corresponding international patent application under the Patent Cooperation Treaty (PCT/CN2026/119506), assigned to Peking University and Shandong Laboratory of Yantai Drug Discovery, covering aspects of the technology described in this manuscript.

Langtaosha (LTS) Preprint doi: https://doi.org/10.65215/LTSpreprints.2026.11.04.000373. This version posted November 4, 2026. The copyright holder for this preprint (which was not certified by peer review) is the author/funder. Creative Commons license: CC Attribution-NonCommercial-NoDerivatives 4.0 https://creativecommons.org/licenses/by-nc-nd/4.0

References

1. Khan, M. I. H., Sawyer, B. J., Akins, N. S. & Le, H. V. A systematic review on the kappa opioid receptor and its ligands: New directions for the treatment of pain, anxiety, depression, and drug abuse. *Eur. J. Med. Chem.* **243**, 114785 (2022).

2. Ortega, A., Blount, J. F. & Manchand, P. S. Salvinorin, a new *trans*-neoclerodane diterpene from *Salvia divinorum* (Labiatae). *J. Chem. Soc. Perkin Trans. 1* **1982**, 2505–2508 (1982).

3. Valdes, L. J. III., Butler, W. M., Hatfield, G. M., Paul, A. G. & Koreeda, M. Divinorin A, a psychotropic terpenoid, and divinorin B from the hallucinogenic Mexican mint, *Salvia divinorum*. *J. Org. Chem.* **49**, 4716–4720 (1984).

4. Roth, B. L. et al. Salvinorin A: A potent naturally occurring nonnitrogenous κ opioid selective agonist. *Proc. Natl Acad. Sci. USA* **99**, 11934–11939 (2002).

5. Yan, F. et al. Identification of the Molecular Mechanisms by Which the Diterpenoid Salvinorin A Binds to κ-Opioid Receptors. *Biochemistry* **44**, 8643–8651 (2005).

6. Béguin, C. et al. Synthesis and in vitro evaluation of salvinorin A analogues: Effect of configuration at C(2) and substitution at C(18). *Bioorg. Med. Chem. Lett.* **16**, 4679–4685 (2006).

7. Hooker, J. M. et al. Pharmacokinetics of the potent hallucinogen, salvinorin A in primates parallels the rapid onset and short duration of effects in humans. *NeuroImage* **41**, 1044–1050 (2008).

8. Vardy, E. et al. A New DREADD Facilitates the Multiplexed Chemogenetic Interrogation of Behavior. *Neuron* **86**, 936–946 (2015).

9. Marchant, N. J. et al. Behavioral and Physiological Effects of a Novel Kappa-Opioid Receptor-Based DREADD in Rats. *Neuropsychopharmacology* **41**, 402–409 (2016).

10. Dykstra, L. A., Gmerek, D. E., Winger, G. & Woods, J. H. Kappa opioids in rhesus monkeys. I. Diuresis, sedation, analgesia and discriminative stimulus effects. *J. Pharmacol. Exp. Ther.* **242**, 413–420 (1987).

11. Wee, S. & Koob, G. F. The role of the dynorphin–κ opioid system in the reinforcing effects of drugs of abuse. *Psychopharmacology* **210**, 121–135 (2010).

12. Land, B. B. et al. The Dysphoric Component of Stress Is Encoded by Activation of the Dynorphin κ-Opioid System. *J. Neurosci.* **28**, 407–414 (2008).

13. Pfeiffer, A., Brantl, V., Herz, A. & Emrich, H. M. Psychotomimesis Mediated by κ Opiate Receptors. *Science* **233**, 774–776 (1986).

14. MacLean, K. A., Johnson, M. W., Reissig, C. J., Prisinzano, T. E. & Griffiths, R. R. Dose-related effects of salvinorin A in humans: dissociative, hallucinogenic, and memory effects. *Psychopharmacology* **226**, 381–392 (2013).

15. Schmidt, M. S. et al. Determination of Salvinorin A in body fluids by high performance liquid chromatography–atmospheric pressure chemical ionization. *J. Chromatogr. B* **818**, 221–225 (2005).

16. Tsujikawa, K. *et al.* In vitrostability and metabolism of salvinorin A in rat plasma. *Xenobiotica* **39**, 391–398 (2009).

17. Roach, J. J. & Shenvi, R. A. A review of salvinorin analogs and their kappa-opioid receptor activity. *Bioorg. Med. Chem. Lett.* **28**, 1436–1445 (2018).

18. Prisinzano, T. E. & Rothman, R. B. Salvinorin A Analogs as Probes in Opioid Pharmacology. *Chem. Rev.* **108**, 1732–1743 (2008).

Langtaosha (LTS) Preprint doi: https://doi.org/10.65215/LTSpreprints.2026.11.04.000373. This version posted November 4, 2026. The copyright holder for this preprint (which was not certified by peer review) is the author/funder. Creative Commons license: CC Attribution-NonCommercial-NoDerivatives 4.0 https://creativecommons.org/licenses/by-nc-nd/4.0

19. Munro, T. A. et al. Standard protecting groups create potent and selective κ opioids: Salvinorin B alkoxymethyl ethers. *Bioorg. Med. Chem.* **16**, 1279–1286 (2008).
20. Riley, A. P. et al. Synthesis and κ-Opioid Receptor Activity of Furan-Substituted Salvinorin A Analogues. *J. Med. Chem.* **57**, 10464–10475 (2014).
21. Scheerer, J. R., Lawrence, J. F., Wang, G. C. & Evans, D. A. Asymmetric Synthesis of Salvinorin A, A Potent κ Opioid Receptor Agonist. *J. Am. Chem. Soc.* **129**, 8968–8969 (2007).
22. Nozawa, M., Suka, Y., Hoshi, T., Suzuki, T. & Hagiwara, H. Total Synthesis of the Hallucinogenic Neoclerodane Diterpenoid Salvinorin A. *Org. Lett.* **10**, 1365–1368 (2008).
23. Hagiwara, H., Suka, Y., Nojima, T., Hoshi, T. & Suzuki, T. Second-generation synthesis of salvinorin A. *Tetrahedron* **65**, 4820–4825 (2009).
24. Line, N. J., Burns, A. C., Butler, S. C., Casbohm, J. & Forsyth, C. J. Total Synthesis of (−)-Salvinorin A. *Chem. Eur. J.* **22**, 17983–17986 (2016).
25. Wang, Y. & Metz, P. Total Synthesis of the Neoclerodane Diterpene Salvinorin A via an Intramolecular Diels–Alder Strategy. *Org. Lett.* **20**, 3418–3421 (2018).
26. Zimdars, P., Wang, Y. & Metz, P. A Protecting-Group-Free Synthesis of (−)-Salvinorin A. *Chem. Eur. J.* **27**, 7968–7973 (2021).
27. Halang, M. & Maier, M. E. Formal Total Synthesis of Salvinorin A. *ChemistryOpen* **11**, e202200015 (2022).
28. Tran, H., McGee, P. & Barriault, L. Formal Synthesis of (±)-Salvinorin A via Gold(I) Catalysis. *Chem. Eur. J.* **29**, e202301640 (2023).
29. Roach, J. J. et al. Dynamic Strategic Bond Analysis Yields a Ten-Step Synthesis of 20-nor-Salvinorin A, a Potent κ-OR Agonist. *ACS Cent. Sci.* **3**, 1329–1336 (2017).
30. Hill, S. J. et al. A Route to Potent, Selective, and Biased Salvinorin Chemical Space. *ACS Cent. Sci.* **9**, 1567–1574 (2023).
31. Han, J. et al. Ligand and G-protein selectivity in the κ-opioid receptor. *Nature* **617**, 417–425 (2023).
32. Zhao, Y. et al. Structural characterization of kappa-opioid receptor dimer in complex with two G proteins. *Nat. Commun.* **17**, 6980 (2026).
33. Li, Z. et al. Decoding the κ Opioid Receptor (KOR): Advancements in Structural Understanding and Implications for Opioid Analgesic Development. *Molecules* **29**, 2635 (2024).
34. Vardy, E. et al. Chemotype-selective Modes of Action of κ-Opioid Receptor Agonists. *J. Biol. Chem.* **288**, 34470–34483 (2013).
35. Vortherms, T. A., Mosier, P. D., Westkaemper, R. B. & Roth, B. L. Differential Helical Orientations among Related G Protein-coupled Receptors Provide a Novel Mechanism for Selectivity. *J. Biol. Chem.* **282**, 3146–3156 (2007).
36. Wang, Y. et al. 2-Methoxymethyl-Salvinorin B Is a Potent κ Opioid Receptor Agonist with Longer Lasting Action in Vivo Than Salvinorin A. *J. Pharmacol. Exp. Ther.* **324**, 1073–1083 (2008).
37. Marcune, B. F., Karady, S., Dolling, U.-H. & Novak, T. J. Methoxymethylation of Alcohols, Phenols, and Avermectin Aglycones Using MOM-2-pyridylsulfide. *J. Org. Chem.* **64**, 2446–2449 (1999).
38. Chen, H. et al. Total Synthesis of (+)-Mutilin: A Transannular [2+2] Cycloaddition/Fragmentation Approach. *J. Am. Chem. Soc.* **144**, 15462–15467 (2022).

Langtaosha (LTS) Preprint doi: https://doi.org/10.65215/LTSpreprints.2026.11.04.000373. This version posted November 4, 2026. The copyright holder for this preprint (which was not certified by peer review) is the author/funder. Creative Commons license: CC Attribution-NonCommercial-NoDerivatives 4.0 https://creativecommons.org/licenses/by-nc-nd/4.0

39. Hoppe, H.-W., Stammen, B., Werner, U., Stein, H. & Welzel, P. An approach to bufadienolides from deoxycholic acid. Reactions of a steroidal αβ-unsaturated aldehyde with some *O*-silylated ketene acetals. *Tetrahedron* **45**, 3695–3710 (1989).

40. Shimo, T., Yasuda, M., Tajima, J. & Somekawa, K. Intramolecular photoreactions of 4-(ω-alkenyloxy)-6-methyl-2-pyrones. *J. Heterocycl. Chem.* **28**, 745–748 (1991).

41. Weber, B. & Seebach, D. Ti-TADDOLate-catalyzed, highly enantioselective addition of alkyl- and aryl-titanum derivatives to aldehydes. *Tetrahedron* **50**, 7473–7484 (1994).

42. Matsuda, A., Ushimaru, T., Kobayashi, Y. & Harada, T. Catalytic Enantioselective Arylation and Heteroarylation of Ketones with Organotitanium Reagents Generated In Situ. *Chem. Eur. J.* **23**, 8605–8609 (2017).

43. Muratspahić, E. et al. Design and structural validation of peptide–drug conjugate ligands of the kappa-opioid receptor. *Nat. Commun.* **14**, 8064 (2023).

44. Doering, N. P. et al. Mechanistic Insights into G Protein-Biased κ-Opioid Receptor Signaling Using Dual-Charged Naltrexamine Amides. *J. Med. Chem.* **69**, 3833–3851 (2026).

45. Uprety, R. et al. Controlling opioid receptor functional selectivity by targeting distinct subpockets of the orthosteric site. *eLife* **10**, e56519 (2021).

46. El Daibani, A. et al. Molecular mechanism of biased signaling at the kappa opioid receptor. *Nat. Commun.* **14**, 1338 (2023).

47. Faridoon, Ng, R., Zhang, G. & Li, J. J. An update on the discovery and development of reversible covalent inhibitors. *Med. Chem. Res.* **32**, 1039–1062 (2023).

48. Leeson, P. D.; Springthorpe, B. The Influence of Drug-like Concepts on Decision-Making in Medicinal Chemistry. *Nat. Rev. Drug Discov.* **6**, 881–890 (2007).

49. Waring, M. J. Lipophilicity in Drug Discovery. *Expert Opin. Drug Discov.* **5**, 235–248 (2010).

50. Fleming, F. F., Yao, L., Ravikumar, P. C., Funk, L. & Shook, B. C. Nitrile-Containing Pharmaceuticals: Efficacious Roles of the Nitrile Pharmacophore. *J. Med. Chem.* **53**, 7902–7917 (2010).

51. Wissner, A. et al. 4-Anilino-6,7-dialkoxyquinoline-3-carbonitrile Inhibitors of Epidermal Growth Factor Receptor Kinase and Their Bioisosteric Relationship to the 4-Anilino-6,7-dialkoxyquinazoline Inhibitors. *J. Med. Chem.* **43**, 3244–3256 (2000).

52. Li, W. et al. Metabolic activation of furan moiety makes Diosbulbin B hepatotoxic. *Arch. Toxicol.* **90**, 863–872 (2016).

53. Kawai, K. et al. Design, synthesis, and structure–activity relationship of novel opioid κ-agonists. *Bioorg. Med. Chem.* **16**, 9188–9201 (2008).

54. Ballesteros, J. A. & Weinstein, H. Integrated methods for the construction of three-dimensional models and computational probing of structure–function relations in G protein-coupled receptors. *Methods in Neurosciences, Vol. 25: Receptor Molecular Biology* 366–428 (Academic Press, 1995).

55. Wang, Y. *et al.* Structures of the entire human opioid receptor family. *Cell* **186**, 413-427.e17 (2023).

56. Meltzer, R. H. *et al.* Electrostatic steering at acetylcholine binding sites. *Biophys. J.* **91**, 1302–1314 (2006).

57. Paton, K. F. et al. The analgesic and anti-inflammatory effects of Salvinorin A analogue β - tetrahydropyran Salvinorin B in mice. *Eur. J. Pain* **21**, 1039–1050 (2017).

58. Le Bars, D., Gozariu, M. & Cadden, S. W. Animal Models of Nociception. *Pharmacol. Rev.* **53**, 597–652 (2001).

Langtaosha (LTS) Preprint doi: https://doi.org/10.65215/LTSpreprints.2026.11.04.000373. This version posted November 4, 2026. The copyright holder for this preprint (which was not certified by peer review) is the author/funder. Creative Commons license: CC Attribution-NonCommercial-NoDerivatives 4.0 https://creativecommons.org/licenses/by-nc-nd/4.0

59. Seelig, A. The Role of Size and Charge for Blood–Brain Barrier Permeation of Drugs and Fatty Acids. *J. Mol. Neurosci.* **33**, 32–41 (2007).

60. Pardridge, W. M. Transport of small molecules through the blood-brain barrier: biology and methodology. *Adv. Drug Deliv. Rev.* **15**, 5–36 (1995).

61. Munro, T. A. et al. Long-acting κ opioid antagonists nor-BNI, GNTI and JDTic: pharmacokinetics in mice and lipophilicity. *BMC Pharmacol.* **12**, 5 (2012).

62. Vauquelin, G. Effects of target binding kinetics on in vivo drug efficacy: k_{off}, k_{on} and rebinding. *Br. J. Pharmacol.* **173**, 2319–2334 (2016).

63. Trapp, S., Rosania, G. R., Horobin, R. W. & Kornhuber, J. Quantitative modeling of selective lysosomal targeting for drug design. *Eur. Biophys. J.* **37**, 1317–1328 (2008).

64. Zürrer, W. E., Wettstein, L., Aicher, H. D., Scheidegger, M. & Ineichen, B. V. The translational potential of salvinorin A: systematic review and meta-analysis of preclinical studies. *Transl. Psychiatry* **15**, 401 (2025).

65. Keasling, A. W. & Zjawiony, J. K. The plant *Salvia divinorum* (Lamiaceae)—chemistry and pharmacology. *Neuropathology of Drug Addictions and Substance Misuse* 551–560 (Elsevier, 2016).

66. Cunningham, C. W., Rothman, R. B. & Prisinzano, T. E. Neuropharmacology of the Naturally Occurring κ-Opioid Hallucinogen Salvinorin A. *Pharmacol. Rev.* **63**, 316–347 (2011).

67. Corey, E. J. & Cheng, X.-M. *The Logic of Chemical Synthesis* (Wiley-Interscience, 1995).

68. Wright, S. C. et al. GLP-1R signaling neighborhoods associate with the susceptibility to adverse drug reactions of incretin mimetics. *Nat. Commun.* **14**, 6243 (2023).

69. Radoux-Mergault, A., Oberhauser, L., Aureli, S., Gervasio, F. L. & Stoeber, M. Subcellular location defines GPCR signal transduction. *Sci. Adv.* **9**, eadf6059 (2023).

70. Klein Herenbrink, C. et al. The role of kinetic context in apparent biased agonism at GPCRs. *Nat. Commun.* **7**, 10842 (2016).

71. Sykes, D. A. et al. The Influence of Receptor Kinetics on the Onset and Duration of Action and the Therapeutic Index of NVA237 and Tiotropium. *J. Pharmacol. Exp. Ther.* **343**, 520–528 (2012).

72. Sykes, D. A. et al. Extrapyramidal side effects of antipsychotics are linked to their association kinetics at dopamine D2 receptors. *Nat. Commun.* **8**, 763 (2017).

73. Wang, X. et al. Antinociceptive and Antipruritic Effects of HSK21542, a Peripherally-Restricted Kappa Opioid Receptor Agonist, in Animal Models of Pain and Itch. *Front. Pharmacol.* **12**, 773204 (2021).

74. Butelman, E. R. & Kreek, M. J. Salvinorin A, a kappa-opioid receptor agonist hallucinogen: pharmacology and potential template for novel pharmacotherapeutic agents in neuropsychiatric disorders. *Front. Pharmacol.* **6**, 190 (2015).

Langtaosha (LTS) Preprint doi: https://doi.org/10.65215/LTSpreprints.2026.11.04.000373. This version posted November 4, 2026. The copyright holder for this preprint (which was not certified by peer review) is the author/funder. Creative Commons license: CC Attribution-NonCommercial-NoDerivatives 4.0 https://creativecommons.org/licenses/by-nc-nd/4.0

Table of Contents

